Volume 1 | Number 1 | Jan 2013 | Pages 1–100

PCCP

Physical Chemistry Chemical Physics
www.rsc.org/pccp

ROYAL SOCIETY OF CHEMISTRY

ROYAL SOCIETY OF CHEMISTRY

www.rsc.org/pccp

ARTICLE TYPE

A theoretical study of the structures and optical spectra of helical copper-silver clusters

Christopher J. Heard[*a] **and Roy L. Johnston**[†a]

The structures and optical response of helical clusters ("Bernal spirals") with compositions $Ag_{12}Cu_1^+$ and $Ag_1Cu_{12}^+$ are calculated within Kohn-Sham density functional theory and the configuration interaction singles variant of time dependent density functional theory. The effects of dopant position within the cluster on the vertical excitation spectrum are investigated according to the underlying electronic structure of the major transitions. The roles of symmetry and geometry are investigated by calculating the optical response of helical, icosahedral and nanorod-like clusters of Ag_{13}^+, finding local structure to be significant in driving the resultant optical response at the subnanometre scale. Further, it is noted that helical clusters have optical properties which are quite distinct from those of nanorods of similar dimensions. The effect of multiple doping is studied by introducing copper atoms into the centre of the silver helix, over the composition range Ag_{13}^+ to $Ag_6Cu_7^+$. There is a complex variation of the major plasmon-like peak over this range, attributed to subtle variations in the influence of the copper 3d band on the excitations and charge transfer for different sites within the cluster. This work suggests that coinage metal nanohelices have unusual, tunable electronic properties, which in addition to their inherent chirality makes them interesting systems of study for chiral catalysis and optoelectronics.

1 Introduction

Helical metal clusters have begun to attract attention from both theoretical and experimental communities. For theoreticians, they provide an interesting model of inherent chirality, with potentially exotic properties which may be studied with computational methods. Recently, Han *et al.* studied the growth of mixed Cu/Ag/Au nanowires and helices inside carbon nanotubes (CNT) using molecular dynamics simulations with embedded atom method (EAM) potentials[1], finding pure and mixed helical structures to be stable within the confined environment, and that both tubes and helices are resilient to changes in metal composition, tube length and CNT dimensions. Posada-Amarillas *et al.* have found these helical species to be locally stable configurations for free $Pd_{12}Pt_1$ clusters during an unbiased energy landscape exploration with the Gupta potential[2]. They characterised the local minima and estimated the rearrangement barriers between helices of various dopant positions and the conversion to the icosahedral global minimum. Gimenez and Schmickler[3] found that twisted, triple stranded bimetallic rods of Au, Ag, Cu and Pd are stable with the EAM, and that surface energy differences

between metals drives the preference for certain permutational isomers.

There is growing evidence that coinage metal clusters may be induced to form twisted nanorods with icosahedral[4] or decahedral[4–6] subunits, implying that various helices based on platonic solids may be created under particular experimental conditions. Kondo and Takayanagi[7] reported helically coiled multishell gold nanorods with a variety of thicknesses down to 0.6 nm (two shells) produced by the electron beam thinning technique. Later, Oshima, Onga and Takayanagi found evidence for single shell gold nanorods comprised of five intertwined strands, with a diameter of 0.4 nm, using the same technique[6]. More recently, Velázquez-Salazar *et al.*[4] produced larger mixed Au-Ag nanorods with wet chemical synthetic methods, finding icosahedral, decahedral and fcc packing in the ratio 7:2:1 respectively. Interestingly, these twisted rods showed fully alloyed compositions of Ag_3Au, which varied little between rods, suggesting particular energetic stability, and a resistance to self-purification. This result shows that for multiply-shelled mixed coinage metal rods, helices may be formed in the absence of strain.

The fact that these helices are found for coinage metals opens the door to optical and catalytic uses, which warrant further study of cluster stability and electronic properties. Coinage metal particles are known on the nanoscale and the subnanoscale to have high efficacy for a range of catalytic reactions, which, particularly for the smaller sizes, are extremely

---

† Electronic Supplementary Information (ESI) available: . See DOI: 10.1039/b000000x/
[a] *School of Chemistry, University of Birmingham, Edgbaston, Birmingham, UK, B15 2TT.*
∗ *Email: cjh085@bham.ac.uk*
† *Email: r.l.johnston@bham.ac.uk*

sensitive to cluster structure and charge state on an atom-by-atom basis. The attractive possibility of introducing chirality, both inherently from the structure and by doping of this class of clusters is a strong motivation for understanding the basic properties of helical metal clusters.

The plasmonic properties of copper [8–12], silver [13–16] and gold particles [14,17–19] as a function of structure and size have been studied extensively for clusters in the nanometre size range. It is well established that gold and copper display weaker, broadened responses relative to silver, and that d→s orbital interband transitions are the cause. Theoretically, the Mie-Drude model works well for large, isotropic particles [17,19,20], whereas time dependent density functional theory (TDDFT) has become a standard method for treating the optical response of particles in the $\leq$ 2 nm range [12,15,18,21–27]. For example, Lang *et al.* [28] combined TDDFT with photodissociation spectroscopy to elucidate the structures of $Au_nCu_{(4-n)}.Ar^+$ clusters. Recently, Shayeghi *et al.* have employed a similar approach for silver and gold cluster cations, using range-corrected TDDFT [24]. Aikens *et al.* [29] calculated the absorption spectra of selected tetrahedral Ag_n clusters $10 \leq n \leq 120$, finding sharp plasmon peaks, whose energies increase linearly with inverse side length. Weissker and Mottet investigated the effect of size and doping of magic number coinage metal clusters in the size range $13 \leq n \leq 147$ [30], observing a broadening and red shift of the response on increasing particle size for each metal. Interestingly, on doping into core-shell geometries, they report a non-monotonic variation of the spectrum, suggesting geometric effects play a complex role in the optical response.

Bernal spirals [31], also known as Boerdijk-Coxeter helices [32] or tetrahelices [33], are chiral clusters comprising chains of face-sharing tetrahedra, with an irrational twist angle between adjacent atoms. Considered originally over half a century ago by geometers and physicists concerned with close-packed structures in liquids [32,34], these exotic species have been investigated more recently both theoretically and experimentally, for colloidal [35,36] and coinage metal [2,4] clusters, and one-dimensional metal halide [37,38] chains.

In this article, we investigate the stabilities and structures of cationic thirteen-atom Bernal spiral clusters of copper and silver, both monometallic and doped with a single atom of the other metal, within the theoretical framework of range corrected DFT and TDDFT. These clusters are chosen to be representative of single walled helical nanoparticles, at a size small enough to allow for high level electronic structure calculations. Bernal spirals may be described as three intertwined helical strands of length 5, 4 and 4 atoms. We investigate the local stability of particular dopant sites and look into the balance of energetic and charge transfer factors responsible. Optical spectra of three geometric motifs, the Bernal spiral, a nanorod-like structure and the icosahedron are simulated and

compared in section 3. In-depth analysis of the electronic excitation spectra of mono-doped cationic coinage metal Bernal spirals is performed in section 4. Finally, in section 5, we consider multiply doped clusters of compositions $Ag_{(13-n)}Cu_n^+$, where n = 1-7, to elucidate the role of dopant loading in the optical response of ultrasmall nanohelices.

2 Computational Details

Right handed tetrahelical clusters were generated according to formula 1 (left handed structures may be produced with a sign inversion in the **j** term). The free parameters are r, which is defined as $\frac{3\sqrt{3}r_0}{10}$, where r_0 is a reasonable coinage metal initial bond length, taken to be 2.69Å, and the height offset h, chosen to be $\frac{1}{\sqrt{10}}$, in accordance with the generation scheme of Chakrabarti and colleagues [39]. The angle between atoms θ is $\arccos(-2/3) \simeq 131.8°$ which gives an irrational twist, ensuring the helix has no rotational repeat unit. The position p_n of atom n is given by the following formula, with the first atom position defined by convention to be at $p_0 = (r, 0, 0)$.

$$p_n = r\cos(n\theta)\mathbf{i} + r\sin(n\theta)\mathbf{j} + nh\mathbf{z} \tag{1}$$

Local geometry optimisation was performed within the plane wave PWscf density functional (DFT) framework, with the Quantum Espresso package [40], utilising ultrasoft RRKJ-type pseudopotentials containing eleven valence electrons per atom. The Methfessel-Paxton smearing scheme [41] was used to aid metallic convergence, with a smearing parameter of 0.002 Ry. The optimisation was considered complete when energies and total forces drop below the respective thresholds of 1×10^{-4} Ry and 1×10^{-3} Ry a_0^{-1}. Densities of state were calculated with an energy grid of spacing 0.001 Ry and projected onto atomic orbital functions. Partial valence charges were calculated with the Bader method [42], localised on atomic sites.

For optical response calculations, local reminimisation of the cluster geometries was performed with the long range corrected LC-ωPBE exchange correlation functional in the atomic orbital based NWCHEM v.6.1 package [43]. This functional has shown recent promise in treating small coinage metal clusters, [24,44] particularly in the reproduction of experimental optical response spectra with TDDFT calculations. This accuracy is attributed to the ability of range corrected functionals to correctly reproduce long-range Coloumb decay, and so perform well for calculations which depend sensitively on this feature. The optical response of coinage metals, where interband transitions and long range charge transfer are a case where this effect is important [27]. A previous study by Shayeghi *et al.* [24] tested a wide range of exchange-correlation functionals for gold and silver tetrameric clusters and found the best agreement with experimental photodepletion spectroscopy to be with the long range corrected PBE functionals LC-ωPBE

and the modified version, LC-ωPBEh[44]. Two basis sets of different quality were utilised, the LANL2DZ basis set and effective core potential (ECP) replacing 10 and 28 electrons per copper and silver atom, respectively, and the higher quality def2-TZVPP basis, with an ECP replacing 10 electrons for copper. The higher level basis was used in sections four and five, where accurate treatments of the electronics are required, and the lower level used in section three, where we are concerned with qualitative comparisons. Both basis sets are tested against each other, giving spectra with good agreement in intensity and linewidth.

Both DFT methods, plane-wave pseudopotential (QE) and atomic orbital basis (NWCHEM), are utilised to ensure the reliability of our calculations across the two calculation methods. The effect of changing method is determined by the relative energies of the clusters in section 4, finding acceptable agreement, despite the change in xc-functional and basis. Because of the importance of range-corrected functionals for optical spectra, the TDDFT spectra are only calculated with NWCHEM, in which the appropriate functionals are available, and therefore all analysis in sections 3, 4.2, 4.3 and 5 in which optical properties are concerned is performed at the NWCHEM level.

After local reminimisation at the appropriate level of theory, which is required to ensure the structures are local minima, the optical spectra of the clusters were simulated from the Kohn-Sham state spectrum within the TDDFT framework, using configuration interaction singles. The spectral calculations were performed for mono-cationic clusters, and so only closed shell electronic configurations are required. By only considering transitions between the spin-allowed singlet states, the calculation of the vertical excitation spectrum is made tractable at the higher level of theory, and allows for a larger number of excited states, and thus a greater range of excitation energies. Analysis of resulting spectra and the electronic composition of transitions is performed using the chemissian software package[45].

3 Cluster geometries

While the optical response converges for larger systems to the isotropic limit, at which the Mie-Drude model accurately predicts the plasmonic behaviour, there is strong evidence that for clusters in the size range we are concerned with, the local geometry makes a significant difference to the electronics, and thus the excitation spectrum[21,22]. Geometric shell closing effects may also have a profound effect[30]. We are therefore interested in decoupling the effects of the cluster composition from its geometry, by considering a range of three structural motifs for the pure silver cluster cation Ag_{13}^+: the tetrahelix, the icosahedron and a nanorod-like cluster with fcc packing, as shown in figure 1. The silver cluster is chosen rather than
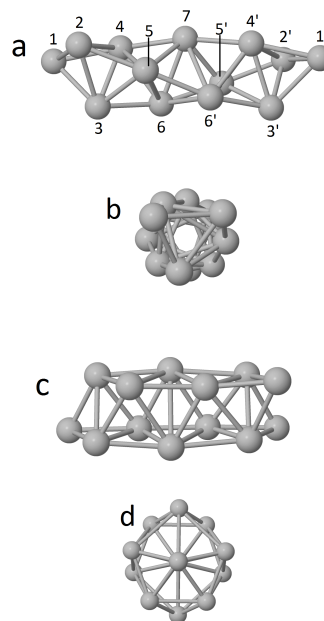

Fig. 1 The structures of the Bernal spiral, shown side-on, with symmetry inequivalent sites labeled 1-7, and their equivalent counterparts labeled with primes (a), the spiral shown end-on (b), fcc rod-like cluster (c) and icosahedron (d). Symmetry inequivalent dopant sites are labeled on the Bernal spiral.

copper in order to avoid the encroachment of d → s interband transitions into the low energy range of the spectrum. The onset of the silver d band is approximately 2 eV higher in energy than for copper[12]. The extent to which this encroachment will occur is likely to depend on structure and so would complicate the analysis. The icosahedron and nanorod-like shapes are chosen due to their high symmetries but significantly different structures. The rod reproduces the aspect ratio of the spiral, whereas the icosahedron is pseudo-spherical in geometry. It should be noted that the icosahedron, while energetically more stable than the helical cluster, is not the global minimum for Ag_{13}. For the neutral cluster, the icosahedron is highly spin-polarized and uncompetitive with the buckled biplanar motif[46,47], and is therefore unlikely to be the global minimum for Ag_{13}^+. Each cluster is generated, the structures locally minimised at the LANL2DZ-ECP level of theory, then the vertical excitation spectrum calculated with TDDFT. Both silver and copper spirals are generated according to formula 1, and thus have identical (artificial) bond lengths of r_0 before relaxation. After local minimisation, the bonds in the spiral are 2.78 ± 0.03 Å along the strands, and nearest neighbours between strands have bond lengths of 2.86 ± 0.11 Å. This compares to very similar intra-strand bond lengths of 2.75 ± 0.15 Å and inter-strand bond lengths of 2.92 ± 0.11 Å in the
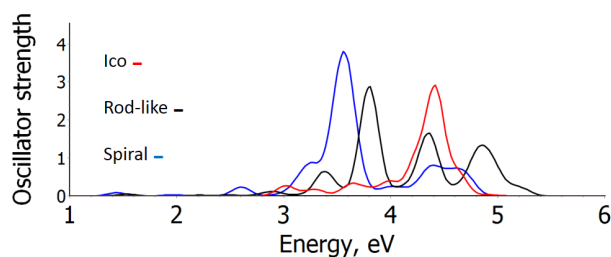
Fig. 2 Double-zeta level optical response spectra of Ag_{13}^+ icosahedral (red), rod-like (black) and Bernal spiral (blue) clusters.

nanorod. For completeness, the bond lengths in the copper helix are 2.45 ± 0.03 Å along the strands and 2.48 ± 0.07 Å between strands.

The spectra are displayed in figure 2 with a Gaussian convolution of 0.2 eV, in order to represent experimental broadening. This convolution does not take into account the effects of coupling between single particle excitations and the plasmonic response, which are noted to affect the fine structure of the peaks[20], but are not calculated within the CIS framework.

In this qualitative description of the spectral response, we consider the broadened features as shown in figure 2, and refer to individual electronic transitions only where relevant. The nanorod-like cluster contains several major excitations centered around 3.4, 3.8, 4.3 and 4.8 eV, the latter three of which contain significant oscillator strength. The multiplicity of the spectrum is due in part to the inequivalence between the long and short axes of the rod. The icosahedron possesses a single large feature at the convolution considered here, at a higher energy than the major peak of the spiral. In fact, this large, broad peak consists of an energetically close-lying set of three strong electronic transitions at energies 4.23, 4.41 and 4.42 eV, and a weaker fourth transition at 4.63 eV. This spectrum agrees well with the results of Harb *et al.*[48], in which the spectrum of the neutral icosahedron is calculated. The experimental results of Baishya *et al.*[49] and TDDFT calculations of Harb *et al.*[26], for neutral Ag_{13} clusters of non-icosahedral, close-packed geometries, also agree reasonably with this result. The supplementary information contains a list of the significantly contributing transitions for the rod-like and icosahedral clusters. The tetrahelix contains three broad features, a small peak around 2.6 eV, a broad, shouldered peak between 3.2 and 3.8 eV, which contains the majority of the oscillator strength, and a region from 4.3 to 5.0 eV. The electronic structure of the

transitions which combine to produce these peaks is investigated in detail in section four, where higher level calculations are performed upon the helix. Qualitatively, we may conclude that the geometry of the cluster makes a great difference to the spectrum, even between the rod and the spiral, whose structures and aspect ratios are similar.

Natural transition orbitals (NTOs)[50] provide an efficient means to combine, in an efficient orbital form, the multiple particle-hole molecular orbital pairs which make up a single excitation in TDDFT calculations. With this method, we may probe the electronic structure of the spectra. For the nanorod, we find that there is a separation in energy scales between longitudinal and transverse excitations, due to the aspect ratio of the cluster. The particle-hole pairs of NTOs for the longitudinal and transverse excitations are given in figure 3, a-b and c-d respectively, and correspond to the most prominent peaks in the spectrum, at 3.8 and 4.3 eV. It is notable that the longitudinal excitation (along the easy axis of the cluster) is at lower energy than the transverse. Thus, the NTO analysis confirms the splitting of the spectrum into a multitude of peaks to be due to a geometric effect, and further, shows there to be some spatial collectivity in the excitation, which is distributed over the entire length of the cluster. The peak at 4.8 eV is due to interband transitions between d and s orbitals. For the icosahedron, there is no splitting of the transition energies according to aspect ratio, and thus there is one major peak region in the spectrum from 4.1 to 4.6 eV. The NTOs which correspond to the largest transition in this region are given in figure 3 e-f and reflect the pseudo-spherical symmetry of the icosahedron.

The NTO pair which contribute most to the major transition for the Bernal spiral are labeled g and h. Similarly to the nanorod, there is a collective oscillation along the easy axis of the cluster, which corresponds to the highest oscillator strength. Higher energy excitations, such as the broad band between 4.3 and 5.0 eV show atom-centric NTOs, for which the hole state is dominated by localised d orbitals, and the particle state is made up of sp orbitals. This is the interband transition expected for high energy excitations, and is depicted in the supplemental information. It is interesting to note that while the structure, bond lengths and qualitative electronic description of the excitations is similar between the rod and helix, the spectra are significantly different.

4 $Ag_{12}Cu_1^+$ and $Ag_1Cu_{12}^+$ helices

On doping from sites 1 to 4, the connectivity of copper increases from 3 to 6, and remains invariant for all further symmetry inequivalent doping sites.

Figure 4 shows the variation of total energy after local minimisation as a function of the dopant position for the monodoped cationic clusters, both at the PWscf-PBE and the reoptimised TZVPP-LC-ωPBE levels. It is clear that the general
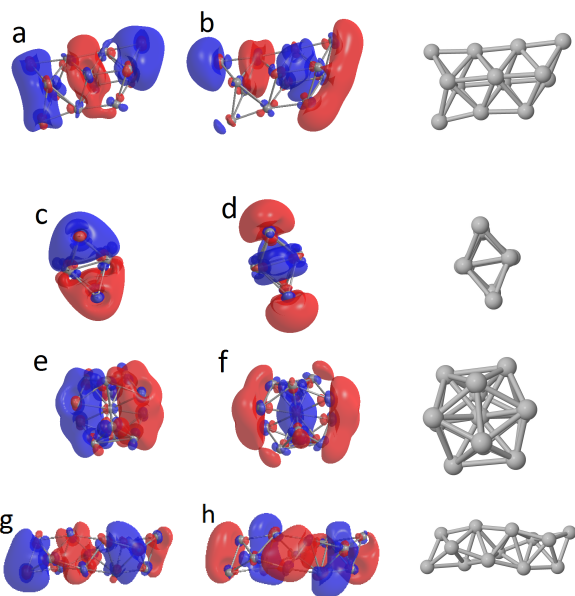
Fig. 3 NTOs for the excitations which make up the dominant peaks in the spectra for Ag_{13}^+. Nanorod NTO pairs are shown for the longitudinal (a-b) and transverse (c-d) excitations. (e-f) are the icosahedral NTOs. (g-h) correspond to the helix geometry. Phases of the orbitals are indicated in red and blue. Diagrams of the underlying structures are given alongside the NTOs.

Fig. 4 Dependence of the energies of the Bernal spiral clusters $Ag_{12}Cu_1^+$ (top) and $Ag_1Cu_{12}^+$ (bottom) on Cu dopant site, at both the TZVPP-LC-ωPBE (green) and PWscf-PBE (red) levels.

trend is for increased stability on doping copper further into the silver cluster, and vice versa for the converse composition. This result is primarily due to geometric concerns. The copper atom has an approximately 13% smaller atomic radius than silver, and thus constrained positions within internal sites are preferred for copper atoms. This is complemented by the fact that copper surfaces have higher surface energies than silver, promoting externalisation of silver atoms. That this surface effect is retained down to the nanoparticle or sub-nanoparticle regime is a result which is observed commonly in the coinage metal literature[3]. An additional factor is the relative binding strengths of homo- and heterometallic bonds. Copper-copper bonds are the strongest, followed by copper-silver, with silver-silver bonds the weakest. Thus in $Ag_1Cu_{12}^+$, the number of copper-silver bonds are minimised, and in $Ag_{12}Cu_1^+$ they are maximised. This trend is clear for the first four dopant sites, for both clusters and at both levels of theory. However, once maximal coordination is reached at site 4, the energetic behaviour becomes more erratic. This fluctuation may be caused by electronic effects, and may be probed by consideration of the charge transfer. For site 6 of $Ag_1Cu_{12}^+$, this erratic behaviour is significant enough that the cluster is no longer a local minimum, converting by a barrierless rearrangement to a distorted fcc-like nanorod structure similar to that of Ag_{13}^+
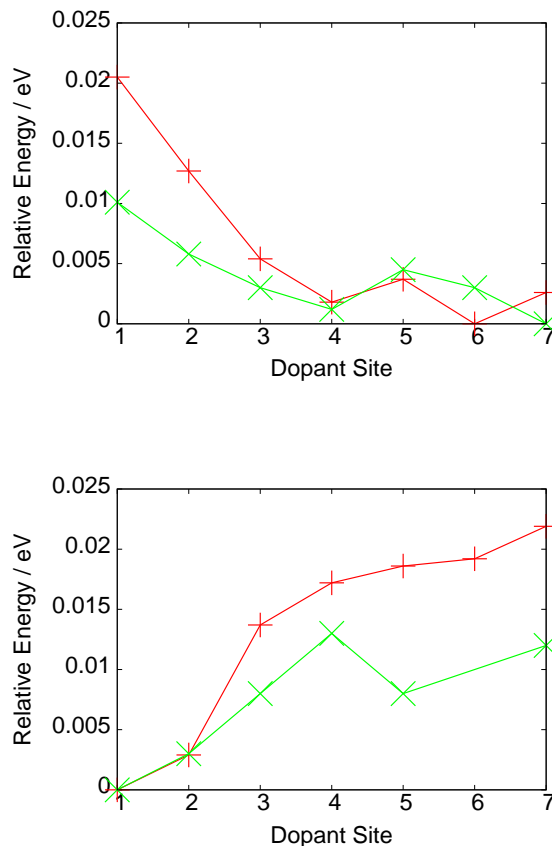
shown in figure 1. This minimum is displayed in the supplementary information.

4.1 Charge transfer

The effect of charge transfer on the energetics of the cluster may arise from direct transfer, in which electropositive atoms donate charge to the more electronegative atoms surrounding it, stabilising both. If charge transfer were a significant effect, it may be expected that energetic stabilisation would be maximised where the dopant atom is surrounded by donors/acceptors of the opposite type. In the case of Ag/Cu systems however, it is not expected that direct transfer is likely to play a significant role. Both atoms have a Pauling electronegativity of 1.9, and previous studies have shown little evidence of this direct transfer[51].

There exists, a second, more subtle effect, due to the geometric constraints of particular positions in the cluster. Indi-
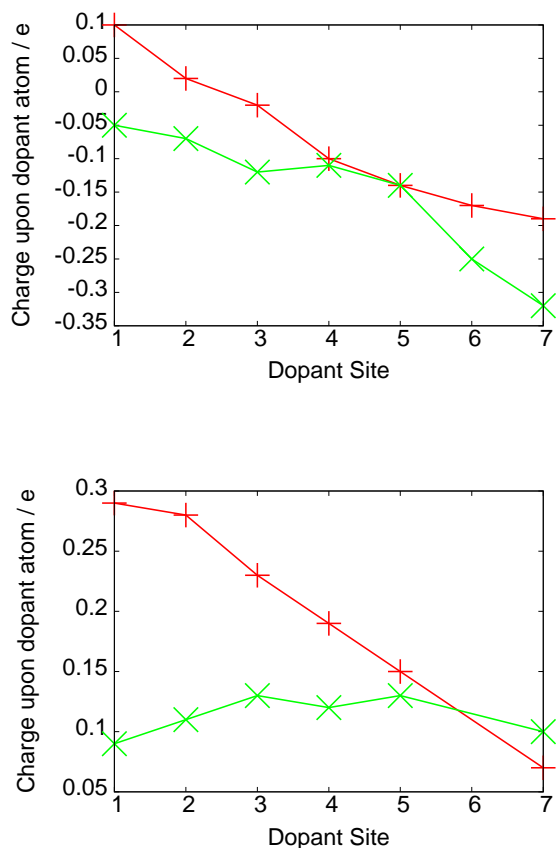
Fig. 5 Bader charge transfer by dopant site for the Bernal spiral clusters $Ag_{12}Cu_1^+$ (top) and $Ag_1Cu_{12}^+$ (bottom). + signs correspond to absolute charge on the dopant atom, × signs correspond to the relative charge transfer after subtraction of the baseline charge for the relevant monometallic cluster. Positive values denote cationic sites.

Site	Charge (Ag_{13}^+) / e	Charge (Cu_{13}^+) / e
1	0.15	0.20
2	0.09	0.17
3	0.10	0.10
4	0.01	0.07
5	0.0	0.02
6	0.08	-0.04
7	0.13	-0.03

Table 1 Inherent charges of each dopant site, for the pure silver and copper clusters.

vidual atomic sites have innate variations in charge due solely to their local geometry, and so provide a "baseline" charge transfer to or from any atom which occupies the site.

To probe these effects, Bader charges are localised upon atomic sites and their values calculated for the monometallic and bimetallic clusters as a function of dopant position. Figure 5 displays, for $Ag_{12}Cu_1^+$ and $Ag_1Cu_{12}^+$, both the total charge accumulation upon the dopant atom for each site (plus signs) and the charge relative to the baseline of the appropriate pure cluster (crosses). For the silver-rich cluster, the copper dopant is a net charge donor when placed in sites 1 or 2. As the dopant moves further into the interior of the cluster, it becomes a net acceptor of charge. The strength and directionality of this charge transfer effect is somewhat surprising. By subtracting the baseline charge, we may isolate the role of the

dopant from the inherent effect of the site. This shows an even stronger charge acceptor behaviour, with transfer of up to 0.32 electrons by site 7. The overall cause of the charge transfer is the copper dopant atom itself, rather than the inherent site charge, which varies in a complex manner over the cluster, as shown in table 1.

For the copper-rich system, there is a similar trend for the overall charge transfer, except that the silver atom is overall positively charged for all site locations. By subtracting the baseline charge, we find the trend is quenched. In effect, all the charge behaviour for copper-rich clusters is due to the geometry of the helix, rather than the silver dopant atom. It is notable that in the absence of site effects (denoted by the green line), the charge on silver is on average +0.11 e/atom, which is very close to the +0.08 e/atom charge expected for a mono-cationic cluster with a uniform charge distribution, and has very little spread about this value.

Overall, copper dopants gain a large amount of negative charge from the surrounding silver, which is maximised by internalisation of the dopant. Silver dopants however, are net charge donors, and have a weak influence on the electronics, varying only by the inherent differences between sites due to the cluster geometry.

4.2 $Ag_{12}Cu_1^+$ spectra

For the silver-rich Bernal spirals, the vertical excitation spectrum is generated with triple-zeta level range-corrected TDDFT for each of the seven symmetry inequivalent dopant sites along with the pure Ag_{13}^+ spiral. When compared to the LANL2DZ spectrum in the previous section, it is apparent that the lower quality basis set performs very well for the pure cluster, with excellent agreement up to around 4.0 eV. This is likely due to the use of accurate xc-functionals. The spectra for each of the dopant sites are given in figure 6, showing no systematic deviation from that of the pure cluster. It is apparent that the response of the mono-doped cluster is qualitatively dominated by the silver. A figure with all spectra overlaid is given in the supplementary information. Analysis of the atomic and orbital makeup of the excitations will determine
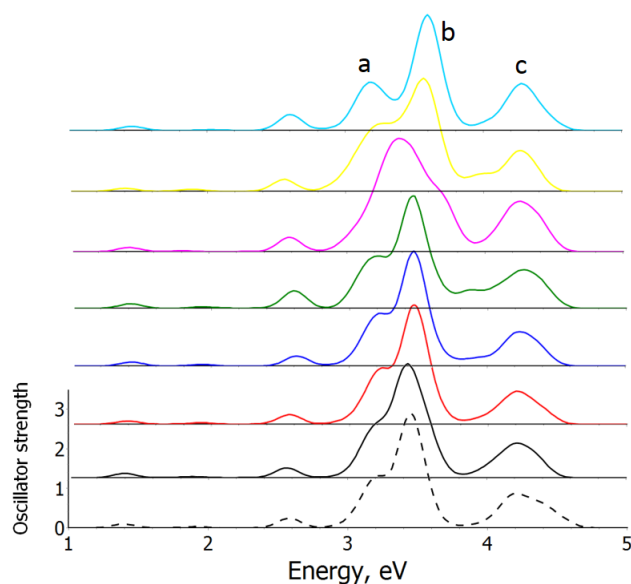
Fig. 6 TDDFT spectra of $Ag_{12}Cu_1^+$ calculated with the def2-TZVPP basis and the LCω-PBE xc-functional. The dashed line corresponds the pure Ag_{13}^+ helix for comparison. From bottom to top - copper dopant in sites 1 to 7. Major peak regions are labelled a, b and c.

Initial orbital	Final orbital	Contribution %	Major transition
126 88.9/9.1/2.0	**134** 34.0/63.4/2.6	**30.3**	s $\rightarrow$ p
126 88.9/9.1/2.0	**133** 31.5/67.3/1.2	**20.7**	s $\rightarrow$ p
126 88.9/9.1/2.0	**131** 65.1/33.9/1.0	**11.5**	s $\rightarrow$ p
123 0.1/0.0/99.9	**129** 82.4/16.5/1.1	**5.92**	d $\rightarrow$ s

Table 2 Major contributing MO pairs (greater than 5%) to the dominant optical excitation in $Ag_{12}Cu_1^+$ with the copper dopant located at site 1, calculated at the def2-TZVPP/LCω-PBE level. The individual atomic orbital contributions to the MO's are provided, according to a Mulliken analysis, along with the overall primary s/p/d electron transfer for each MO pair.

the role of the copper in the electronic structure.

The spectra possess three main peak regions, at around 2.6 eV (a), with low oscillator strength, a semi-continuous, shouldered region from approximately 3.0 to 3.8 eV (b), which varies slightly between dopant sites and contains the majority of the oscillator strength, and a smaller region above 4.0 eV (c). The second peak region corresponds to the "plasmon-like" part of the spectrum, due to its dominance of the oscillator strength and its continuous nature, but given the small size of the cluster, and the multitude of peak regions, the spectrum is possibly more accurately described as being composed of molecule-like excitations. The presence of the silver plasmon peak down to the sub-nanoscale range is a matter of some debate, but irrespective of nomenclature, the spectra agree qualitatively with those of Harb *et al.* for Ag_{13}. As is common for vertical excitation spectra, not only do the peak regions correspond to several excitations, but each excitation is of multi-reference nature. Therefore, for the "plasmonic" region in the spectrum, we take the excitation which has the great oscillator strength as representative of that peak, and consider the transitions which make up a significant proportion of that excitation. Table 2 shows the MOs which contribute more than 5% to the largest peak, and the individual contributions they make for an example case, where the copper dopant occupies site 1.

We observe that for the three prominent MO pairs, which all start from orbital HOMO-2 (MO 126), the overall transfer is from s to p, with little involvement of d orbitals, which agrees very well with the recent result of Shayeghi and coworkers

for smaller cationic silver clusters[24]. This also agrees with the results of Harb *et al.*[26], who observe transitions predominantly of s or d character, to s+p character in neutral, matrix-embedded Ag_n clusters for $12 \leq n \leq 22$. Their analysis, based on the depletion of orbitals during the transition suggests that the increased s-d mixing in larger silver clusters causes a greater contribution of d orbitals to the initial state, which play a significant role by $n=20$.

The fourth most prominent contribution is clearly of a different character, originating largely from the d orbitals of the copper dopant atom, providing a strongly Cu d to Ag s transition. This band is the cause of the difference between the spectrum of the doped cluster and the pure silver system, and is the key to the differences between spectra from the various dopant sites, where the copper more or less effectively contributes to intermetallic, interband transitions. Figure 7 shows a typical plot of the projected density of states around the Fermi energy for the mono-doped, silver rich cluster. We observe that the HOMO and LUMO have s/p ratios of approximately 2 and 1, respectively, in agreement with the previous analysis. There is no significant effect of dopant site upon the HOMO energy, nor the HOMO-LUMO gaps, because this region is dominated by silver character, as previously noted. However, the d band edge is changed in a complex manner with dopant position. We find that there is a variation of up to 0.6 eV, with the overall trend that the more stable and highly coordinated dopant sites induce a shift of the d band closer in energy to the HOMO, thus giving the copper interband transition an increased influence in the excitations. As a result, the more highly coordinated copper atoms not only stabilise the cluster through geometric effects, but have an extra influence on the electronics, by more effectively shifting the d band into the optically and chemically relevant region. This variable d band is the primary cause of the complex variation we find in the spectra. Additional DOS plots, for both $Ag_{12}Cu_1^+$ and $Cu_{12}Ag_1^+$ are given in the supplementary information for comparison.

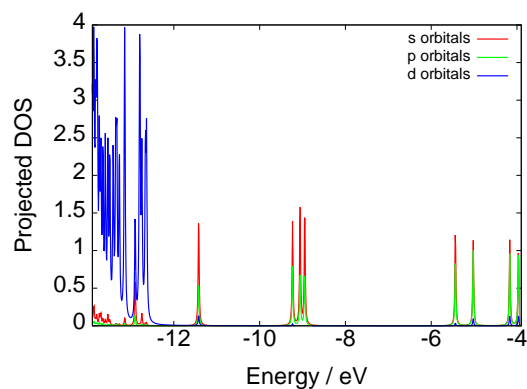**Fig. 7** Representative density of states plot, projected onto s, p and d orbitals for $Ag_{12}Cu_1^+$ with the dopant at site 1. The HOMO is at -8.9 eV, as depicted by the vertical black line. Also shown is the edge of the d band which begins at -12.3 eV.
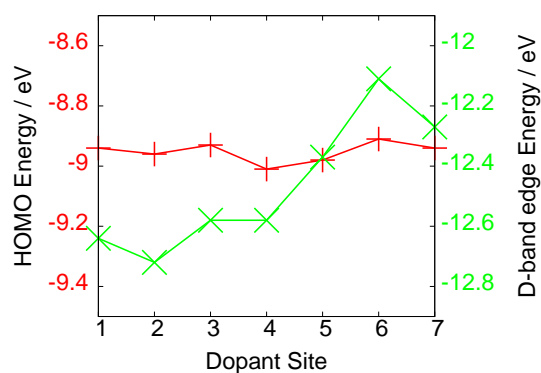

Fig. 8 Variation of the d band edge ($\times$) and HOMO (+) energies for each dopant site of $Ag_{12}Cu_1^+$.

4.3 $Ag_1Cu_{12}^+$ spectra

The spectra for the dopant sites of the $Ag_1Cu_{12}^+$ spirals are calculated analogously to the silver-rich clusters. The number of excited states required to reproduce the spectrum is much larger than for $Ag_{12}Cu_1^+$ as the spectrum is more continuous in its composition, and thus are generated for the smaller range of 0 eV to 3.8 eV, which is nevertheless sufficient to reproduce the major response features. This is noted by Lecoultre *et al.*,[12] for copper clusters up to Cu_9, in which transitions occur over the full range of energies studied.

The results are shown for selected dopant sites in figure 9, displaying a very broad, shouldered peak region, which, anal-
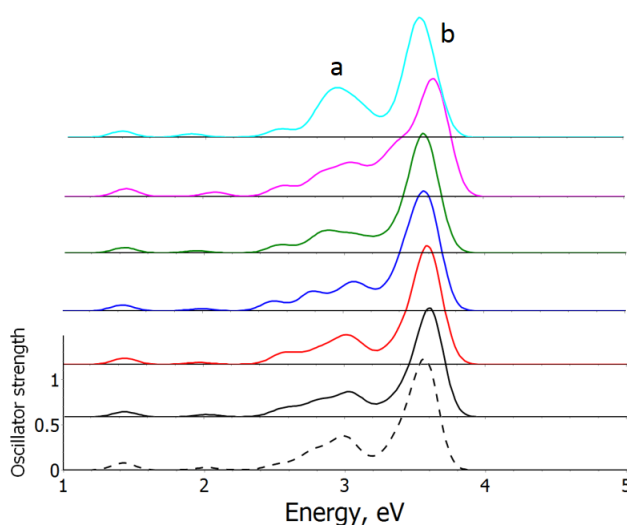

Fig. 9 TDDFT spectra of $Ag_1Cu_{12}^+$ calculated with the def2-TZVPP basis and the LC-ωPBE xc-functional. The dashed line corresponds to the pure Cu_{13}^+ helix for comparison. From bottom to top silver dopant in sites 1 to 7 (site 6 is absent). Major peak regions are labelled a and b.

ogously to the silver-rich regime, does not vary systematically with dopant position. The peaks, labelled a and b are separated into a semi-continuous band, ranging approximately from 2.8 to 3.2 eV and a higher intensity region centered at 3.6 eV. The maximum combined oscillator strength is around 1.5; significantly lower in intensity than for $Ag_{12}Cu_1^+$, in line with the well known result that copper exhibits a less pronounced optical response than silver. The reason for this diminished response is the interference of the 5d electrons. Interband transitions in copper appear in the same energy range as the plasmon response, damping and broadening the plasmon peak. This effect becomes more pronounced the smaller the cluster, so that nanometre scale copper clusters are often found to have no plasmonic behaviour.

Table 3 shows the MO pairs and their Mulliken populations projected upon atomic orbitals of transition b, for all MO pairs which provide greater than 4% of the intensity. This value is chosen because the peaks are of an even more highly multi-reference nature than for the silver-rich clusters, and as such, individual MO pairs contribute less to the transition. It is found that the first and third largest contributions are due to d to s transfer, with hole orbitals predominantly from the copper 5d band and particle states in the copper 6s band. The second most prominent transition is largely s-like in character, both for the hole and particle states, though the overall transfer is still from d orbitals to s orbitals. Resolving the MOs by atom type for this second MO pair, we find that this transi-

Initial orbital	Final orbital	Contribution %	Major transition
162 3.8/2.0/94.1	**185** 83.4/9.8/6.9	**4.8**	$d \rightarrow s$
181 74.7/8.6/16.7	**188** 87.9/8.7/3.4	**4.3**	$d \rightarrow s$
144 5.9/1.2/92.9	**184** 76.6/10.2/13.2	**4.2**	$d \rightarrow s$

Table 3 Major contributing MO pairs (greater than 4%) to the dominant optical excitation in $Ag_1Cu_{12}^+$ with the silver dopant located at site 1, calculated at the TZVPP/LC-ωPBE level. The individual atomic orbital contributions to the MO's are provided, according to a Mulliken analysis, along with the overall primary s/p/d electron transfer for each MO pair.

tion contains a significant proportion of silver. The electrons are distributed 85% on copper and 15% on silver for the hole state and 83% copper / 17% silver for the particle state, which is considerably larger in silver proportion than the $\simeq$ 12% of electrons contributed to the system in total by the silver atoms. The d orbitals involved in significant electronic transitions are contributed solely by copper atoms, and the s orbitals predominantly from silver atoms.

Overall, we find that in the silver-rich case, the copper contributes d→s transitions, due to the involvement of the energetically high-lying copper d band, thus affecting both the position and oscillator strength of the response. Conversely, in the copper-rich case, which is dominated by the d→s transitions, the silver s-orbitals contribute to the response, subtly affecting the peak positions.

5 Multiple dopants

Weissker and Mottet found that there is a non-monotonic, non-trivial variation of the optical response on doping for core-shell silver-gold and silver-copper clusters[30]. It was observed that the $Ag_{32}Au_6$ cluster exhibited an excitation spectrum different from, and not intermediate between Ag_{38} and Au_{38}, and thus that the core may play a strong modulating role. For $Ag_{32}Cu_6$, they observed a dramatic reduction in oscillator strength compared to the pure silver cluster. In order to probe whether this effect is found for helical systems, we generate multiply doped cationic clusters $Ag_{(13-x)}Cu_x^+$. By systematically replacing silver atoms with copper, radiating outward from the central site (site 7) in the order 7, 6, 6', 5, 5', etc., we produce compositions up to the approximate 50:50 composition $Ag_6Cu_7^+$. Absorption spectra are produced at the triple zeta level for each composition, as shown in figure 10.

There are three main excitation regions in the doping series spectra, labelled a, b and c. It is clear that for peaks a and b, there is a systematic red shift on increased copper doping. Peak b shows the variation from a shoulder on the pure silver cluster spectrum, to a separate peak for the pure copper. For each additional copper dopant, this peak shifts to the red, and becomes increasingly damped and separate from peak c. Peak c is the major resonance, for both pure clus-
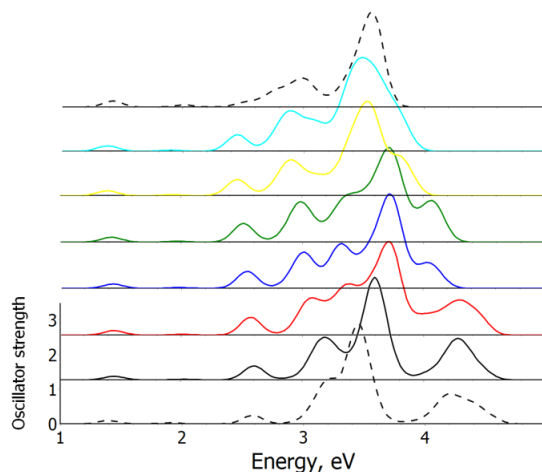

Fig. 10 TDDFT spectra of $Ag_{(13-x)}Cu_x^+$ (x = 0-7 and 13), calculated with the def2-TZVPP basis and the LC-ωPBE xc-functional. Bottom to top are Ag_{13}^+ to Cu_{13}^+. Both pure spirals are included for comparison.

ters and every intermediate dopant level. Qualitatively, it is of note that this peak becomes increasingly damped as copper loading increases. From Ag_{13}^+ to $Ag_{10}Cu_3^+$, the main resonance is blueshifted, but from $Ag_{10}Cu_3^+$ to $Ag_6Cu_7^+$ it becomes systematically redshifted. Overall, this variation spans a range of around 0.3 eV, and would potentially be detectable in experiment. As observed in section four, the central site causes a much more significant blue shift of the major peak in $Ag_{12}Cu_1^+$ than other sites, which is attributed to charge transfer effects. The present doping series introduces copper atoms radiating outwards from the centre (site 7), and thus the inherent differences between sites, along with the trend to move from silver to copper responses causes this unusual trend. Overall, there is no clear establishment of a core effect as found in ref. 30, which is likely due to high symmetry geometric shell closing effects. The current spectral series shows a systematic variation in oscillator strength and peak position between pure silver and copper, though the individual peak positions vary in a complex manner.

It is found that over the entire range of compositions, there is no significant change in the atomic orbital contribution to MOs relevant to the transitions, the position of the MOs near to the Fermi energy or the HOMO-LUMO gap. However, there is a monotonic shift of the d band to higher energies on increasing copper loading. The d band edge shifts by up to 0.2 eV, with a smaller effect observed in the less significant d orbital at higher energy. We conclude that the cause of the overall spectral shift from silver to copper is, as in the case of

changing copper dopant position in $Ag_{12}Cu_1^+$, predominantly a result of the increasing contribution of the copper interband transitions to the excitations. A plot of the density of states around the energy of the copper d-band for each dopant level is given in the supplementary information.

6 Conclusions

We have undertaken a systematic study into the effects of structure, dopant position and doping level on the optical response behaviour of thirteen-atom Bernal spiral coinage metal clusters containing silver and copper. By probing the underlying electronic structure, from the point of view of charge transfer, the orbital compositions of transitions, and the contributions to the important excitations of each metal, we have determined the causes of the major peaks in the absorption spectra and their variations. We conclude that the effect of dopant position is minor for sub-nanometre Bernal spirals, but that increased dopant loading causes a noticeable and systematic shift due primarily to the copper d-band edge encroaching on the chemically relevant orbital range. We expect this to prove useful for the rational design of chiral nanoclusters with specific chemical and electronic properties. Work is ongoing to investigate the significant difference in optical properties between helical and related rod-like clusters.

7 Acknowledgments

References

1 Han Y., Zhou J., Dong J., and Yoshiyuki K. Formation of single-walled bimetallic coinage alloy nanotubes in confined carbon nanotubes: molecular dynamics simulations. *Phys. Chem. Chem. Phys.*, 15:17171–17178, 2013.

2 Pacheco-Contreras R., Dessens-Félix M., Borbón-González D. J., Paz-Borbón L. O., Johnston R. L., Schön J. C., and Posada-Amarillas A. Tetrahelix Conformations and Transformation Pathways in Pt_1Pd_{12} Clusters. *J. Phys. Chem. A*, 116:5235–5239, 2012.

3 Giménez M. C. and Schmicker W. Monte Carlo simulation of nanowires of different metals and two-metal alloys. *J. Chem. Phys.*, 134:064707, 2011.

4 Velázquez-Salazar J. J., Esparza R., Mejía-Rosales S. J., Estrada-Salas R., Ponce A., Deepak F. L., Castro-Guerrero C., and José-Yacamán M. Experimental Evidence of Icosahedral and Decahedral Packing in One-Dimensional Nanostructures. *ACS Nano*, 5(8):6272–6278, 2011.

5 González J. C., Rodrigues V., Bettini J., Rego L. G. C., Rocha A. R., Coura P. Z., Dantas S. O., Sato F., Galvão D. S., and Ugarte D. Indication of Unusual Pentagonal Structures in Atomic-Size Cu Nanowires. *Phys. Rev. Lett.*, 93(12):126103, 2004.

6 Oshima Y., Onga A., and Takayanagi K. Helical Gold Nanotube Synthesized at 150 K. *Phys. Rev. Lett.*, 91(20):205503, 2003.

7 Kondo Y. and Takayanagi K. Synthesis and Characterization of Helical Multi-Shell Gold Nanowires. *Science*, 289:606–608, 2000.

8 Wang H., Tam F., Grady N. K., and Halas N. J. Cu Nanoshells: Effects of Interband Transitions on the Nanoparticle Plasmon Resonance. *J. Phys. Chem. B Lett.*, 109(39):18218–18222, 2005.

9 Pedersen D. B. and Wang S. Surface Plasmon Resonance Spectra of 2.8 ± 0.5 nm Diameter Copper Nanoparticles in Both Near and Far Fields. *J. Phys. Chem. C*, 111:17493–17499, 2007.

10 Chan G. C., Zhao J., Hicks E. M., Schatz G. C., and Van Duyne R. P. Plasmonic Properties of Copper Nanoparticles Fabricated by Nanosphere Lithography. *Nano Lett.*, 7(7):1947–1952, 2007.

11 Bigot J-Y., Merle J-C., Cregut O., and Daunois A. Electron Dynamics in Copper Metallic Nanoparticles Probed with Femtosecond Optical Pulses. *Phys. Rev. Lett.*, 75(25):4702–4706, 1995.

12 Lecoultre S., Rydlo A., Felix C., Buttet J., Gilb S., and Harbich W. Optical absorption of small copper clusters in neon: Cu_n, (n=1-9). *J. Chem. Phys.*, 134(7):074303, 2011.

13 Jensen T. R., Malinsky M. D., Haynes C. L., and Van Duyne R. P. Nanosphere Lithography: Tunable Localized Surface Plasmon Resonance Spectra of Silver Nanoparticles. *J. Phys. Chem. B*, 104(45):10549–10556, 2000.

14 Link S. and El-Sayed S. A. Spectral properties and relaxation dynamics of surface plasmon electronic oscillations in gold and silver nanodots and nanorods. *J. Phys. Chem. B*, 103(40):8410–8426, 1999.

15 Lecoultre S., Rydlo A., Buttet J., Felix C., Gilb S., and Harbich W. Ultraviolet-visible absorption of small silver clusters in neon: Ag_n (n=1-9). *J. Chem. Phys.*, 134(18):184504, 2011.

16 Tiggesbäumker J., Köller L., Lutz H. O., and Meiwes-Broer K. H. Giant resonances in silver-cluster photofragmentation. *Chem. Phys. Lett.*, 190(1):42–47, 1992.

17 Alvarez M. M., Khoury J. T., Schaaff T. G., Shafigullin M. N., Vezmar I., and Whetten R. L. Optical Absorption Spectra of Nanocrystal Gold Molecules. *J. Phys. Chem. B*, 101:3706–3712, 1997.

18 Lecoultre S., Rydlo A., Felix C., , Buttet J., Gilb S., and Harbich W. UV-visible absorption of small gold clusters in neon: Au_n (n=1-5 and 7-9). *J. Chem. Phys.*, 134(7):074302, 2011.

19 Palpant B., Prével B., Lermé J., Cottancin E., Pellarin M., Treilleux M., Perez A., Vialle J. L., and Broyer M. Optical properties of gold clusters in the size range 2-4 nm. *Phys Rev. B*, 57(3):1963–1970, 1998.

20 de Heer W. The physics of simple metal clusters: experimental aspects and simple models. *Rev. Mod. Phys.*, 65(3):611–676, 1993.

21 Lozano X-L., Barron H., Mottet C., and Weissker H-Ch. Aspect-Ratio and Size-Dependent Emergence of the Surface-Plasmon Resonance in Gold Nanorods- an *ab initio* TDDFT Study. *Phys. Chem. Chem. Phys.*, 16(5):1820–1823, 2014.

22 Gilb S., Jacobsen K., Schooss D., Furche F. Ahlrichs A., and Kappes M. M. Electronic photodissociation spectroscopy of Au_n^+.Xe (n=711) versus time-dependent density functional theory prediction. *J. Chem. Phys.*, 121(10):4619–4627, 2004.

23 Schweizer A., Weber J. M., Gilb S., Schneider H., Schooss D., and

Kappes M. M. Electronic photodissociation spectroscopy of $Au_4^+ \cdot Ar_n$, n=0-4: Experiment and theory. *J. Chem. Phys.*, 119(7):3699–3710, 2003.

24 Shayeghi A., Johnston R. L., and Schäfer R. Evaluation of photodissociation spectroscopy as a structure elucidation tool for isolated clusters: a case study of Ag_4^+ and Au_4^+. *Phys. Chem. Chem. Phys.*, 15(45):19715–23, 2013.

25 Tiago M. L., Idrobo J. C, Öğüt S., Jellinek J., and Chelikowsky J. R. Electronic and optical excitations in Ag_n clusters (n=1-8): Comparison of density-functional and many-body theories. *Phys. Rev. B*, 79(15):155419, 2009.

26 Harb M., Rabilloud F., Simon D., Rydlo A., Lecoultre S., Conus F., Rodrigues V., and Félix C. Optical absorption of small silver clusters: Ag_n, (n=4-22). *J. Chem. Phys.*, 129:194108, 2008.

27 Rabilloud F. UV-visible absorption spectra of metallic clusters from TDDFT calculations. *Eur. Phys. J. D.*, 67(18), 2013.

28 Lang S. M., Claes P., Cuong N. T., Nguyen M. T., Lievens P., and Janssens E. Copper doping of small gold cluster cations: Influence on geometric and electronic structure. *J. Chem. Phys.*, 135:224305, 2011.

29 Aikens C. M., Li S., and Schatz G. C. From Discrete Electronic States to Plasmons: TDDFT Optical Absorption Properties of Ag_n (n=10, 20, 35, 56, 84, 120) Tetrahedral Clusters. *J. Phys. Chem. C.*, 112:11272–11279, 2008.

30 Weissker H-Ch. and Mottet C. Optical properties of pure and core-shell noble-metal nanoclusters from TDDFT: The influence of the atomic structure. *Phys. Rev. B*, 84(16):165443, 2011.

31 Bernal J. D. The structure of liquids. *Proc. R. Soc. London A*, 280:299–322, 1964.

32 Coxeter H. S. M. *Regular Complex Polytopes*. Cambridge University Press, 1st edition, 1974.

33 Buckminster-Fuller R. *Synergetics*. Macmillan, 1975.

34 Boerdijk A. H. Some Remarks Concerning Close-Packing of Equal Spheres. *Phillips Res. Rep.*, 7(4):303–313, 1952.

35 Campbell A. I., Anderson V. J., van Duijneveldt J. S., and Bartlett P. Dynamical Arrest in Attractive Colloids: The Effect of Long-Range Repulsion. *Phys. Rev. Lett.*, 94:208301, 2005.

36 Sciortino F., Tartagli P., and Zaccarelli E. One-Dimensional Cluster Growth and Branching Gels in Colloidal Systems with Short-Range Depletion Attraction and Screened Electrostatic Repulsion. *J. Phys. Chem. B*, 109(46):21942–21953, 2005.

37 Hartl H. $(cO(CP)_2)(CuI_2)_n$ (n = 3, 4), Cobaltocenium Iodocuprates(1) with Unusual Anion Structures. *Angew. Chem. Int. Ed.*, 26(9):927–928, 1987.

38 Zheng C., Hoffman R., and Nelson D. R. A Helical Face-Sharing Tetrahedron Chain with Irrational Twist, Stella Quadrangula, and Related Matters. *J. Am. Chem. Soc.*, 112:3784–3791, 1990.

39 Morgan J. W., Chakrabarti D., Dorsatz N., and Wales D. J. Designing a Bernal spiral from patchy colloids. *ACS Nano*, 7(2):1246–1256, 2013.

40 Giannozzi P., Baroni S., Bonini N., Calandra M., Car R., Cavazzoni C., Ceresoli D., Chiarotti G. L., Concoccioni M., Dabo I., Dal Corso A., de Gironcoli S., Fabris S., Fratesi G., Gebauer R., Gerstmann U., Gougoussis C., Kokalj A., Lazzeri M., Martin-Samos L., Marzari N., Mauri F., Mazzarello R., Paolini S., Pasquarello A., Paulatto L., Sbraccia C., Scandolo S., Sclauzero G., Seitsonen A. P., Smogunov A., Umari P., and Wentcovitch R. M. QUANTUM ESPRESSO: A modular and open-source software project for quantum simulations of materials. *J. Phys.: Condens. Matter*, 21:395502, 2009.

41 Methfessel M. and Paxton A. T. High-Precision Sampling for Brillouin-Zone Integration in Metals. *Phys. Rev. B.*, 40(6):3616–3621, 1989.

42 Tang W., Sanville E., and Henkelman G. A grid-based Bader analysis algorithm without lattice bias. *J. Phys.: Condens. Matter*, 21(8):084204, 2009.

43 Valiev M., Bylaska E. J., Govind N., Kowalski K., Straatsma T. P., van Dam H. J. J., Wang D., Nieplocha J., Apra E., Windus T. L., and de Jong W. A. NWchem: a comprehensive and scalable open-source solution for large scale molecular simulations. *Comput. Phys. Commun.*, 181:1477–1489, 2010.

44 Rohrdanz M. A., Martins K. M., and Herbert J. M. A long-range-corrected density functional that performs well for both ground-state properties and time-dependent density functional theory excitation energies, including charge-transfer excited states. *J. Chem. Phys.*, 130:054112, 2009.

45 Skripnikov L. A computer program to analyse and visualise quantum-chemical calculations. 2012.

46 Longo R. C. and Gallego L. J. Structures of 13-atom clusters of fcc transition metals by *ab initio* and semiempirical calculations. *Phys. Rev. B.*, 74:193409, 2006.

47 Barron H., Fernández-Seivane L., Weissker H-Ch., and López Lozano X. Trends and Properties of 13-Atom Ag-Au Nanoalloys I: Structure and Electronic Properties. *J. Phys. Chem. C.*, 117:21450–21459, 2013.

48 Harb M., Rabilloud F., and Simon D. Structural, electronic, magnetic and optical properties of icosahedral silver-nickel nanoclusters. *Phys. Chem. Chem. Phys.*, 12:4246–4254, 2010.

49 Baishya K., Idrobo J. C., Öğüt S., Yang M., Jackson K., and Jellinek J. Optical absorption spectra of intermediate-size silver clusters from first principles. *Phys. Rev. B.*, 78:075439, 2008.

50 Martin R. L. Natural transition orbitals. *J. Chem. Phys.*, 118(11):4775–4777, 2003.

51 Heard C. J. and Johnston R. L. A density functional global optimisation study of neutral 8-atom Cu-Ag and Cu-Au clusters. *Eur. Phys. J. D.*, 67(34):30601–30607, 2013.

Optical response spectra of $Ag_nCu^+_{13-n}$ Bernal spiral clusters show subtle variations by dopant site and loading. Comparison to nanorod-like and icosahedral clusters shows local geometry plays a significant role in electronic transitions at the sub-nanoscale.
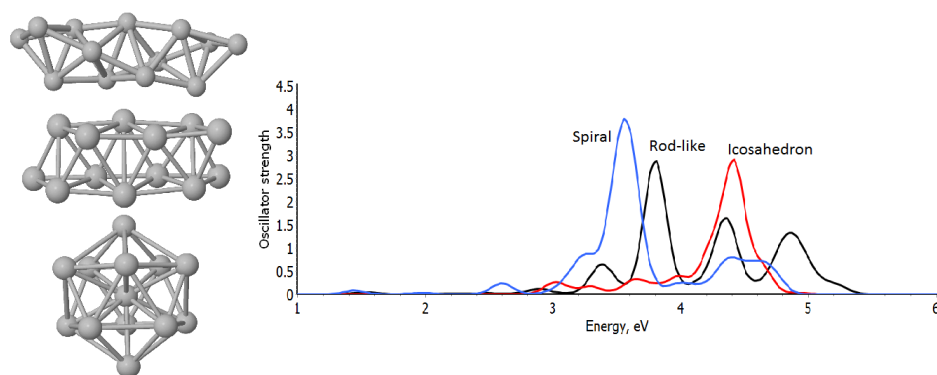

Figure 1:

1